

Q-Band MMW Transmission Enabled by Joint Probabilistic Shaping and Precoding With MZM-Based OCS Modulation

Hengxin Yan, Jiaohao Bi , Dong Guo , Xinying Li, Xiaolong Pan, Hongwu Ge, Wei Wu, Chao Yu, Xiangjun Xin, Qi Zhang , Member, IEEE, Ran Gao , Haipeng Yao , Senior Member, IEEE, Ze Dong , Zhipei Li , Huan Chang, and Sitong Zhou

Abstract—In this letter, we propose a novel and straightforward scheme for Q-band (33–50 GHz) millimeter-wave signal generation enabled by a Mach-Zehnder modulator (MZM)-based joint algorithm, which combines probabilistic shaping (PS) and precoding technology, to enhance the anti-interference ability of the transmission system. Based on the proposed scheme, we experimentally demonstrate the generation and transmission of 1.4-Gbaud 46-GHz PS-16-quadrature-amplitude-modulation (PS-16QAM) vector signals, showcasing improved bit-error-ratio (BER) in both standard single-mode fiber (SSMF) and wireless transmission cases. The proposed scheme exhibits a clear advantage in terms of nonlinear interference suppression and satisfies the hard-decision forward-error-correction (HD-FEC) threshold with a BER of 3.8×10^{-3} in radio-over-fiber (RoF) systems.

Index Terms—Millimeter-wave (MMW), radio-over-fiber (RoF), probabilistic shaping (PS), precoding.

I. INTRODUCTION

INCREASING demand for mobile data traffic and high-definition (HD) services has led to a growing need for increased bandwidth in fifth-generation (5G) radio access networks. Millimeter-wave technology has gathered more and more attention due to its vast available bandwidth and ability to support high data rates [1], [2], [3]. High-speed millimeter-wave

signals can be generated by using photonic-aided millimeter-wave systems, which can also facilitate fiber-wireless integration transmission. The photonic-aided radio-over-fiber (RoF) technique has been proposed to deliver millimeter-wave signals at high frequencies, and a considerable amount of literature has been published on photonic vector mm-wave signal generation [2], [3], [4], [5]. Although these schemes only employ one Mach-Zehnder modulator (MZM), the precoding technique considerably reduces the Euclidean distance of the transmitter constellation, hence restricting the transmission distance [6], [7]. In order to improve the signal-to-noise ratio (SNR), increasing the optical power into the photodetector (PD) for high-power electrical millimeter-wave signal generation is necessary for a long transmission distance. However, the high input power will restrict the system's performance due to the saturation of the optoelectronics. Predictably, the system performance will improve if the saturation nonlinearity can be appropriately compensated.

Nonlinearity compensation and constellation equalization are two major areas of communication research in recent years. Probabilistic shaping (PS) is a common algorithm used to compensate for nonlinearity distortion [8], [9], [10], [11]. PS technique stands out among other algorithms due to its ability to achieve fine rates and closely approach ultimate performance by bridging the shaping gap. Through the use of time superposition, PS enables the realization of the Maxwell-Boltzmann distribution by sending each quadrature amplitude modulation (QAM) symbol with a unique probability. Compared with normal uniform constellations, PS reduces the average power and source entropy, leading to better system performance in terms of near-Shannon performance. It is well known that the PS scheme can reduce the transmitted power that has influence on the introduced nonlinear distortion. It has been demonstrated that the usage of PS significantly enhances transmission performance with extended distance and increased capacity [10], [11], [12], [13]. Over the past decade, the PS has been well verified to be able to bring significant performance gains with extended distance or increased capacity. Many different PS schemes have been proposed in the literatures and their performance improvement has also been verified.

In this letter, we propose a novel scheme for generating a high-frequency PS-16QAM vector radio-frequency (RF) signal. The

Manuscript received 28 March 2023; revised 15 April 2023; accepted 17 April 2023. Date of publication 24 April 2023; date of current version 16 June 2023. This work was supported in part by the Funding National Natural Science Foundation of China under Grants U22A2087, 62105027, and 62205023, in part by the National Science Fund for Excellent Young Scholars under Grant 62022016, and in part by the Beijing Institute of Technology Research Fund Programs for Young Scholars under Grant XSQD-202205011. (*Corresponding authors:* Dong Guo; Xinying Li.)

Hengxin Yan, Jiaohao Bi, Dong Guo, Xinying Li, Xiaolong Pan, Chao Yu, Xiangjun Xin, Ran Gao, Ze Dong, Zhipei Li, Huan Chang, and Sitong Zhou are with the Beijing Institute of Technology, Beijing 100811, China (e-mail: 3120210821@bit.edu.cn; lofoten@yeah.net; guodong@bit.edu.cn; xinying@bit.edu.cn; panxiaolong@bit.edu.cn; yuchao_bit@163.com; xinxianjun@bit.edu.cn; 6120190142@bit.edu.cn; zdong9@bit.edu.cn; lizhipei@bit.edu.cn; changhuan@bit.edu.cn; 7520210121@bit.edu.cn).

Qi Zhang and Haipeng Yao are with the School of Electronic Engineering, Beijing University of Posts and Telecommunications, Beijing 100876, China (e-mail: zhangqi@bupt.edu.cn; yaohaipeng@bupt.edu.cn).

Hongwu Ge and Wei Wu are with the Chinese Electronics Technology Group 54th Institute Shijiazhuang, Hebei 100846, China (e-mail: 13731120962@139.com; weiwu0696@sina.com).

Digital Object Identifier 10.1109/JPHOT.2023.3269560

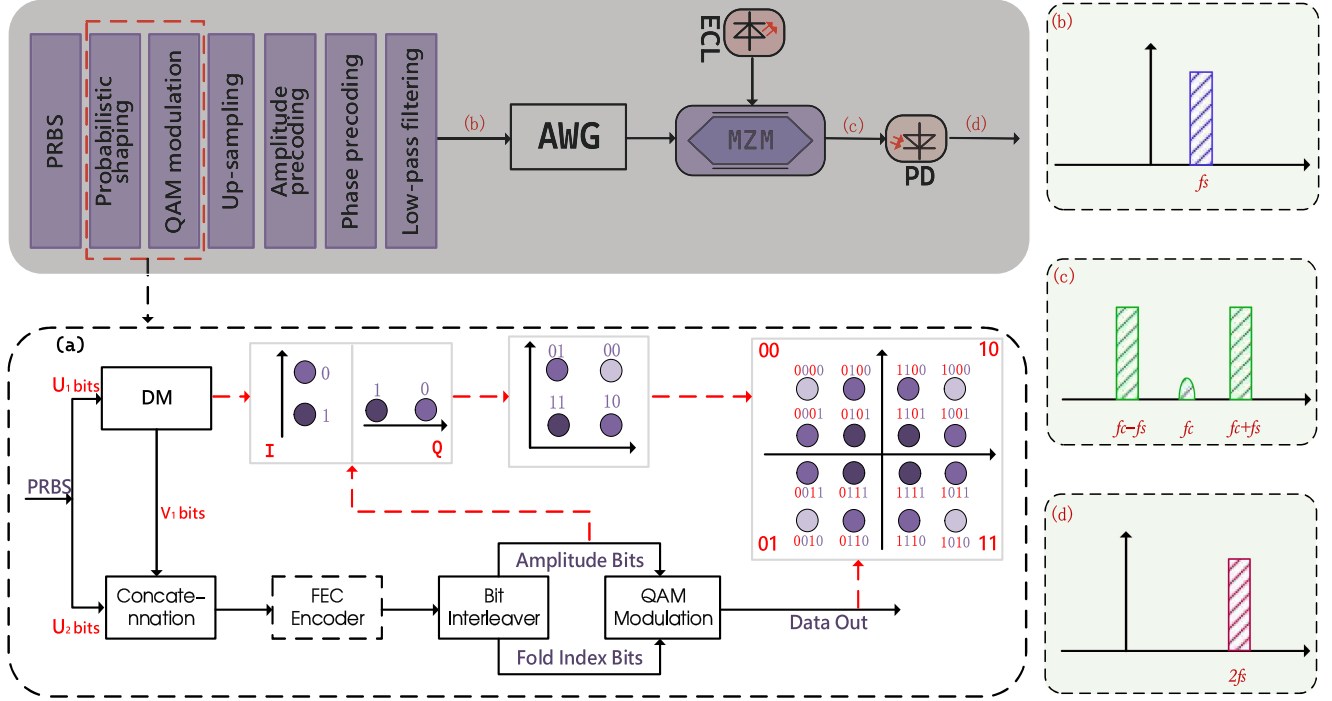


Fig. 1. The principle of photonic PS-16QAM vector signal at frequency f_s . (a) Scheme diagram of generating the PS-16QAM signals. (b) Schematic spectrum of driving electrical PS-16QAM vector signal. (c) Schematic spectrum of photonic PS-16QAM vector signal after passing through the MZM. (d) Schematic spectrum of the received signal after the PD. ECL: external cavity laser, MZM: Mach-Zehnder modulator, PD: photodiode.

system generates photonic vector signals at Q-band enabled by MZM-based optical carrier suppression (OCS) technique. The driving (RF) signal, carrying multi-amplitude QAM transmitter data, is optimized through a joint optimization algorithm, incorporating PS and precoding techniques. The proposed scheme has significantly enhanced bit-error-ratio (BER) performance in both standard single-mode fiber (SSMF) and wireless transmission scenarios. Experimental results demonstrate that the joint optimization algorithm can efficiently improve the system performance, with all BERs meeting the hard-decision forward error correction threshold (HD-FEC) of 3.8×10^{-3} .

II. PRINCIPLE

Fig. 1 illustrate the generation procedure of photonic vector RF signal at the frequency of f_s which carries the electrical quadrature amplitude modulation data. The signal has undergone shaping through the utilization of a distribution matcher (DM) and a precoding module.

Fig. 1(a) depicts the schematic representation of generating the PS-16QAM signals. After the module, the mapping of QAM modulation, and up-sampling, the resulting constellation points in the PS-QAM format display a distribution that follows the Maxwell-Boltzmann distribution, which can be respectively expressed as [11]

$$\begin{aligned} P_X(x_i) &= \frac{1}{\sum_{k=1}^M e^{-v|x_k|^2}} e^{-v|x_i|^2} \quad (x_i \\ &= a_m + b_n j; a_m, b_n = \pm 1, \pm 3;) \end{aligned} \quad (1)$$

Where v is a scaling factor that can be adjusted to change the information entropy and achieve rate-adaptation.

The principle of probabilistic fold shaping (PFS) scheme is a technique that can be used to actualize N-fold rotationally symmetrical QAM formats, specifically the 4-fold symmetrical 16-QAM format [14]. The scheme operates by first converting the PRBS into the PS module. And then the signal is divided into two branches consisting of U_1 and U_2 bits. U_1 bits on the upper branch are transmitted into DM to generate the non-uniformly distribution for different amplitude. The output of the DM is represented by V_1 symbols. In order to generate the PS-16QAM format that follows the Maxwell-Boltzmann distribution, the probability of V_1 symbols should satisfy

$$P_A(a_m) = \frac{1}{\sum_{k=1}^{\sqrt{M}/2} e^{-va_k^2}} e^{-va_m^2} \quad (a_m = 1, 3) \quad (2)$$

Therefore, we have

$$P_A(a_m) * P_A(b_n) = P_X(x_i) \quad (x_i = a_m + b_n j) \quad (3)$$

As Fig. 1 shows, V_1 bits converted from V_1 non-uniformly distributed symbols are concatenated with U_2 original bits, which have a uniform distribution. The resulting sequence is then encoded using Forward Error Correction (FEC) encoding, which guarantees the absence of bit errors at the receiving end. The encoded sequence, consisting of uniformly distributed parity check bits and U_2 information bits, is utilized as the fold index bits, providing symmetry for the symbol mapping. Meanwhile, V_1 information bits converted from non-uniformly distributed symbols are used as amplitude bits. These bits pass through a bit-interleaver, which divides them into two branches to change the

amplitude distribution of I and Q. The non-uniformly distributed points are indicated by different colors, each representing a different probability. Finally, the fold index bits and amplitude bits are combined in Quadrature Amplitude Modulation (QAM) and transformed into a sequence of symbols with Maxwell-Boltzmann distribution, resulting in the PS-16QAM format. It is essential to highlight that FEC encoding plays a crucial role in ensuring the integrity of the data before it reaches the distribution de-matcher at the receiving end.

After the PS module, the precoding approach is then used to process the signal and ensure that the PD output signal is a signal at frequency f_s can be expressed as

$$E_{RF}(t) = K_1(t) \sin[2\pi f_s t + \varphi(t)]. \quad (4)$$

Where K_1 and φ denote the amplitude and phase of the driving RF signal at frequency f_s , respectively. K_1 has a variety of values since the transmitter data adopts multi-amplitude vector modulation.

Assuming that the continuous-wavelength (CW) light wave emitted by an external cavity laser (ECL) with the center frequency of f_c has constant amplitude K_2 and can be expressed as

$$E_{CW}(t) = K_2 \exp(j2\pi f_c t). \quad (5)$$

The MZM is biased at its minimal transmission point to implement OCS modulation by adjusting the DC bias voltage. The two first-order subcarriers from the MZM can be expressed as

$$\begin{aligned} E_{MZM}(t) = & 2jK_2 \{ J_{-1}(k) \exp[j2\pi(f_c - f_s)t - j\varphi t] \\ & + J_{+1}(k) \exp[j2\pi(f_c + f_s)t - j\varphi t] \} \end{aligned} \quad (6)$$

Where $J_{-1}(\cdot)$ and $J_{+1}(\cdot)$ is the Bessel function of the first kind. k is equal to $\pi V_{\text{drive}} K_1(t)/V_\pi$, while V_{drive} and V_π , denote driving voltage and half-wave voltage of the MZM, respectively. The (6) demonstrates that the MZM generates two first-order subcarriers that are spaced by $2f_s$. Fig. 1(c) shows the schematic output spectrum of the MZM.

At the receiver, the incoming signal is directly fed into the PD. After the square-law PD conversion, the output current of the PD can be expressed as

$$i_{RF}(t) = \frac{1}{2} R J_1^2(k) \cos[2\pi \cdot 2f_s t + 2\varphi(t)] \quad (7)$$

Where R denotes the PD sensitivity. According to Fig. 1(d), we can see from (7) that the frequency $2f_s$ of the obtained RF signal is double of the driving RF signal (f_s).

Based on the frequency doubling scheme [15], the frequency of the output signal change to $2f_s$, and the corresponding phase turns to be $2\varphi(t)$ shown by (7). Additionally, the amplitude of the output signal is carried by the term of the square of $J_1(k)$, which depends on the ratio of V_{drive} to V_π . The amplitude K_1 and phase φ of the driving RF signal should satisfy

$$K_{data} = J_1^2(\pi K_1 V_{\text{drive}} / V_\pi); \varphi_{data} = 2\varphi \quad (8)$$

Where K_{data} and φ_{data} respectively denote the amplitude and phase of the original transmitter data. For the 16QAM transmitter data, the obtained value of amplitude K_1 and phase

φ by resolving (8) are just the precoded amplitude and phase which can be assigned to the driving RF signal.

III. EXPERIMENT AND RESULT

To validate the proposed scheme, a simulation was conducted to generate PS-16QAM vector signals with PD direct detection. At the transmitter, a precoded 8-GHz vector signal, carrying 0.5-Gbaud PS-16QAM data, was generated by MATLAB programming and then uploaded into an arbitrary waveform generator (AWG) with 128-GSa/s sampling rate, to implement digital-to-analog conversion (DAC). Then, using an MZM driven at its minimum transmission point, the analog signal was utilized to modulate the CW output from an ECL. To set the specified optical signal-to-noise ratio (OSNR), the output from the MZM was passed through a device that can add depolarized noise to the input signal. After that, the resulting optical signal was fed into a PD. The signal underwent additional processing at the receiver's DSP module, including down-converting, down-sampling, and de-mapping.

The BER performance of the traditional and PS-precoded 16QAM signals is shown in Fig. 3. The results demonstrate that, in the range of interest for OSNR, the PS-precoded 16QAM signal outperforms the traditional 16QAM signal in terms of BER. When the OSNR is about 13 dB, the error rate of the probabilistic shaping system falls below the HD-FEC threshold. Compared with the traditional 16QAM system, the OSNR requirement for reaching a BER of HD-FEC threshold is 1 dB lower in the proposed PS-precoded system. This indicates that the proposed integration scheme can provide reliable information transmission by utilizing standard HD-FEC. The simulation results demonstrate that the proposed scheme has superior anti-interference capabilities and a reduced BER value.

The experiment setup, employing the 1-m wireless or 3-km SSMF and 1-m wireless transmission of a 46-GHz RF signal, is depicted in Fig. 2. The electrical PS-16QAM vector signal is generated in MATLAB with the code length is 32768 bit and then loaded into an arbitrary waveform generator (AWG) with 92 Gsa/s sampling rate. The power-amplified vector signal drives the 40 GHz bandwidth of MZM, which is biased at its minimum transmission point to enable OCS modulation, to modulate the continuous wave from the ECL. Fig. 2(a) and (b) illustrate the optical spectra of the normal 16QAM and PS-16QAM signals after they pass through the MZM, respectively. The optical signal is then amplified by an Erbium-doped fiber amplifier before being transmitted over either a 3-km SSMF or directly to a PD. The optical-to-electrical (O/E) conversion is implemented by a 50-GHz PD. EA2 amplifies the detected signal at 46-GHz, which is subsequently sent to a rectangular horn antenna operating in the 22–50-GHz frequency range. After 1-m wireless transmission, an identical rectangular horn antenna receives the mm-wave signal, which is then amplified by a low-noise electrical amplifier (EA3). To perform the analog-to-digital conversion, the signal is captured by a digital storage oscilloscope (OSC) with 128-GSa/s sampling rate and subsequently processed via offline DSP comprised of down-conversion, resampling, constant modulus algorithm (CMA), blind phase search (BPS), decision-directed

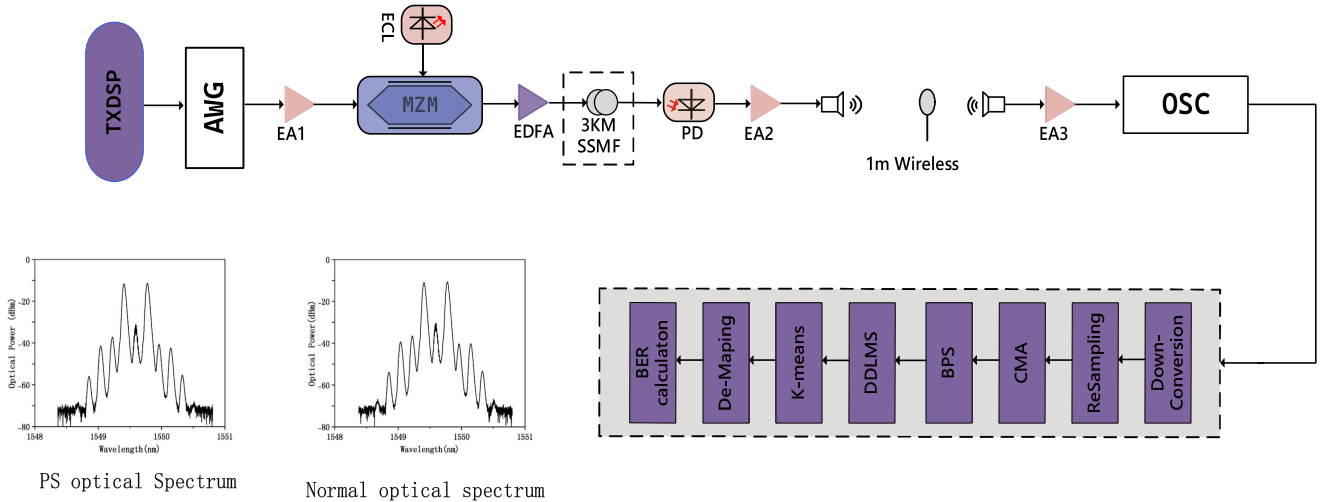


Fig. 2. Experimental setup. EA: electrical amplifier, EDFA: erbium-doped fiber amplifier.

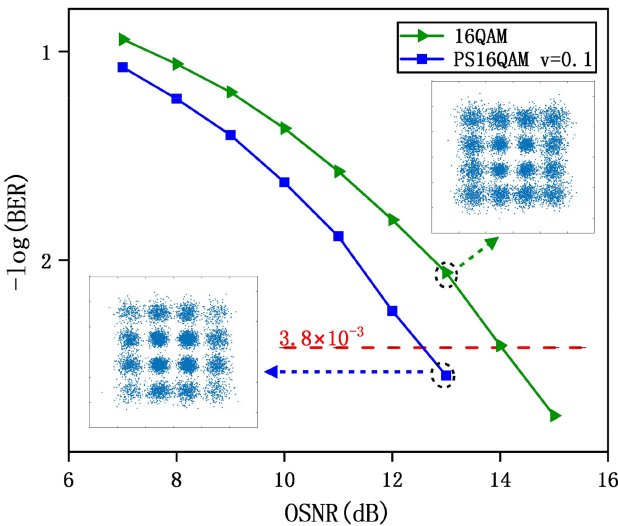


Fig. 3. Simulated BER versus the OSNR.

least mean square (DDLMS), K-means clustering algorithm, De-Mapping, and final BER calculation.

Fig. 4 compares the BER performance of three different transmission scenarios. The results demonstrate the feasibility of the system, as both normal 16QAM and PS-16QAM can achieve a BER performance below the SD-FEC threshold with a power input higher than -3 dBm. Conversely, in the absence of PS, the BER performance is hardly reduced below the HD-FEC threshold. However, for the cases with PS, the BER performance is consistently maintained at an acceptable level and is effectively reduced below the HD-FEC threshold. These results highlight the superiority of probabilistic shaping in improving BER performance. Compared with the fixed probability distribution of tradition constellation, under the condition that the minimum Euclidean distance in the constellation remains unchanged, PS greatly reduces the average power of the constellation, improving the anti-interference ability of the transmission system. The results demonstrate that the PS technique can

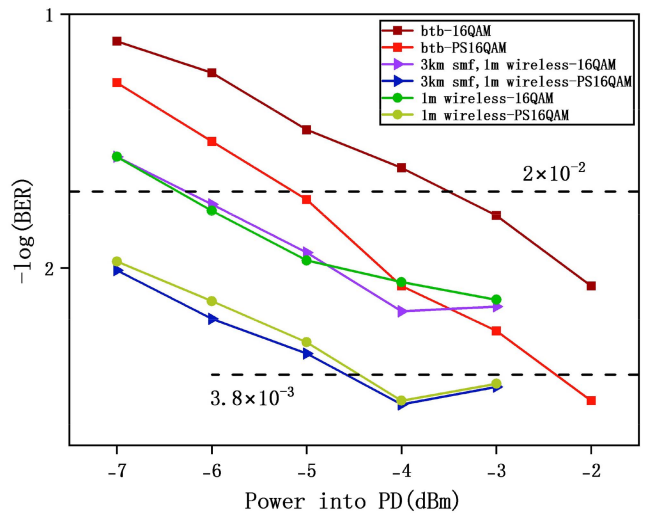


Fig. 4. Measured BER versus the power into PD.

effectively alleviate the nonlinear effects of signals in the RoF systems.

Fig. 4 demonstrates that the BER of Back-to-Back (BTB) systems is consistently higher compared to the other systems. This can be attributed to the saturation of optoelectronics caused by the high input power. The received constellations at -4 dBm and -5 dBm are presented in Fig. 5. Due to energy loss in the transmission link, the constellations of the latter two systems exhibit superior performance, resulting in a better BER. The sixteen clusters in the constellations are well separated, demonstrating the effectiveness of the precoding technology and the DSP algorithm at the receiver. The clearness of the PS-16QAM constellation diagram indicates that the improved BER performance is a result of the joint algorithm. The probability distribution of the PS-16QAM constellation points successfully achieves the goal of having dense low-energy points and sparse high-energy points, while maintaining the minimum Euclidean distance in the constellation.

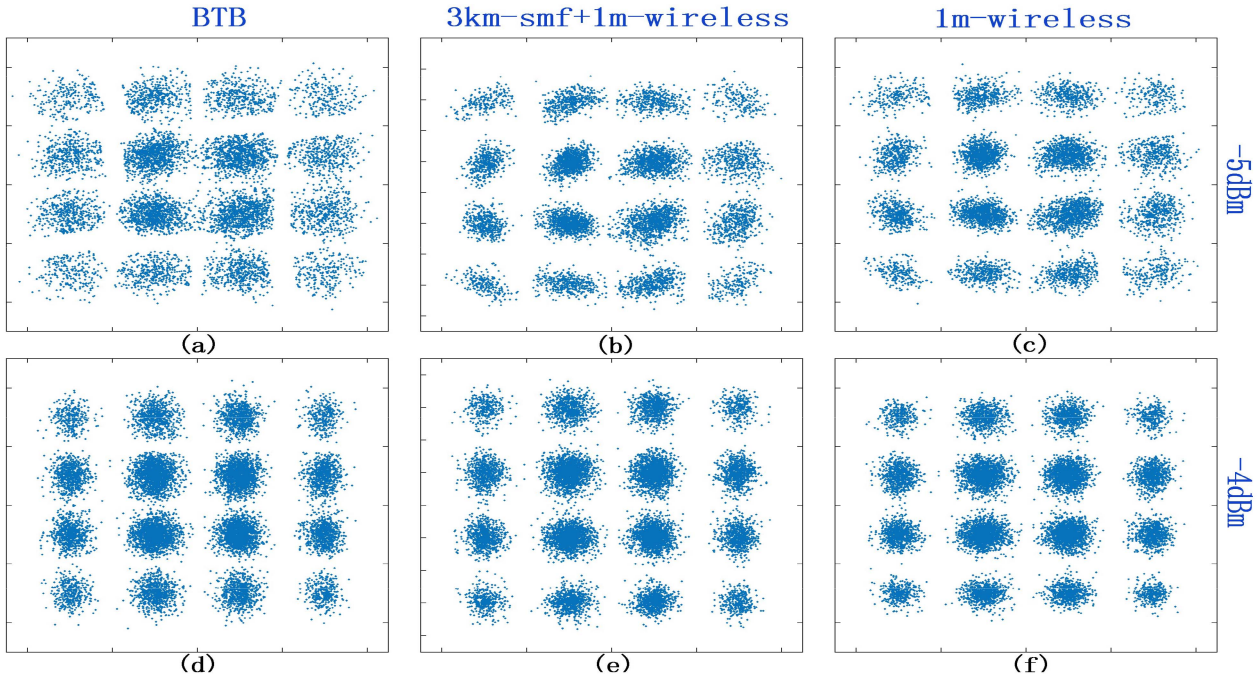


Fig. 5. Received constellations of PS-16QAM after different transmission cases. The power into PD is -5 dBm : (a) BTB, (b) 3 km-smf+1 m-wireless, (c) 1 m-wireless. The power into PD is -4 dBm : (d) BTB, (e) 3 km-smf+1 m-wireless, (f) 1 m-wireless.

IV. CONCLUSION

In conclusion, we propose a novel joint algorithm based on PS and precoding technology for multi-amplitude QAM vector signals in the mm-wave band. The proposed scheme leverages the MZM-based OCS modulation to generate the 1.4-Gbaud 16QAM and PS-16QAM vector signals at 46 GHz. The experimental results demonstrate that, the BER of the PS-16QAM vector signal can be maintained below the HD-FEC threshold of 3.8×10^{-3} after fiber-wireless integration transmission. The results of our experiments indicate that the proposed scheme is capable of effectively compensating for nonlinearity distortion and can support longer distances with increased input optical power into the PD.

REFERENCES

- [1] T. P. McKenna, J. A. Nanzer, and T. R. Clark, "Experimental demonstration of photonic millimeter-wave system for high capacity point-to-point wireless communications," *J. Lightw. Technol.*, vol. 32, no. 20, pp. 3588–3594, Oct. 2014.
- [2] W. Li et al., "OFDM-PS-256QAM signal delivery at 47.45 Gb/s over 4.6-kilometers wireless distance at the W band," *Opt. Lett.*, vol. 47, no. 16, pp. 4072–4075, 2022.
- [3] X. Li et al., "Delivery of 54-gb/s 8QAM W-band signal and 32-Gb/s 16QAM K-band signal over 20-km SMF-28 and 2500-m wireless distance," *J. Lightw. Technol.*, vol. 36, no. 1, pp. 50–56, Jan. 2018.
- [4] L. Zhao, J. Yu, L. Chen, P. Min, J. Li, and R. Wang, "16QAM vector millimeter-wave signal generation based on phase modulator with photonic frequency doubling and precoding," *IEEE Photon. J.*, vol. 8, no. 2, Apr. 2016, Art. no. 5500708.
- [5] J. Ding et al., "Wireless transmission of a 200-m PS-64QAM THz-wave signal using a likelihood-based selection radius-directed equalizer," *Opt. Lett.*, vol. 47, no. 15, pp. 3904–4907, 2022.
- [6] L. Chen, R. Deng, J. He, Q. Chen, Y. Liu, and C. Xiang, "W-band vector signal generation by photonic frequency quadrupling and balanced precoding," *IEEE Photon. Technol. Lett.*, vol. 28, no. 17, pp. 1807–1810, Sep. 2016.
- [7] J. Xiao, Z. Zhang, X. Li, Y. Xu, L. Chen, and J. Yu, "High-frequency photonic vector signal generation employing a single phase modulator," *IEEE Photon. J.*, vol. 7, no. 2, pp. 1–6, Apr. 2015.
- [8] D. Semrau et al., "Achievable information rates estimates in optically amplified transmission systems using nonlinearity compensation and probabilistic shaping," *Opt. Lett.*, vol. 42, no. 1, pp. 121–124, 2017.
- [9] B. Liu, X. Li, Y. Zhang, X. Xin, and J. Yu, "Probabilistic shaping for ROF system with heterodyne coherent detection," *APL Photon.*, vol. 2, no. 5, 2017, Art. no. 056104.
- [10] S. Zhou, X. Liu, R. Gao, Z. Jiang, H. Zhang, and X. Xin, "Adaptive Bayesian neural networks nonlinear equalizer in a 300-Gbit/s PAM8 transmission for IM/DD OAM mode division multiplexing," *Opt. Lett.*, vol. 48, no. 2, pp. 464–467, 2022.
- [11] J. Cho and P. J. Winzer, "Probabilistic constellation shaping for optical fiber communications," *J. Lightw. Technol.*, vol. 37, no. 6, pp. 1590–1607, Mar. 2019.
- [12] J. Shi et al., "Probabilistically shaped 1024-QAM OFDM transmission in an IM-DD system," in *Proc. Opt. Fiber Commun. Conf. Expo.*, 2018, pp. 1–3.
- [13] J. Wei et al., "Probabilistic shaping and neural network-based optimization for a nonlinear frequency division multiplexing system," *Opt. Lett.*, vol. 46, no. 15, pp. 3697–3700, 2021.
- [14] J. Ding, J. Zhang, Y. Wei, F. Zhao, C. Li, and J. Yu, "Comparison of geometrically shaped 32-QAM and probabilistically shaped 32-QAM in a bandwidth-limited IM-DD system," *J. Lightw. Technol.*, vol. 38, no. 16, pp. 4352–4358, Aug. 2020.
- [15] X. Li et al., "QAM vector signal generation by optical carrier suppression and precoding techniques," *IEEE Photon. Technol. Lett.*, vol. 27, no. 18, pp. 1977–1980, Sep. 2015.